AIMS Materials Science, 4(4): 991-1009.
DOI: 10.3934/matersci.2017.4.991
Received: 27 June 2017
Accepted: 03 September 2017
Published: 07 September 2017

http://www.aimspress.com/journal/Materials

Research article

Synthesis and electrocatalytic properties of $La_{0.8}Sr_{0.2}FeO_{3-\delta}$ perovskite oxide for oxygen reactions

R.A. Silva [1], C.O. Soares [2], R. Afonso [2], M.D. Carvalho [3], A.C. Tavares [4], M.E. Melo Jorge [3], A. Gomes [3], M.I. da Silva Pereira [5], and C.M. Rangel [1,*]

[1] Laboratório Nacional de Energia e Geologia, LNEG, Paço do Lumiar 22, 1649-038 Lisboa, Portugal
[2] Centro de Ciências Moleculares e Materiais, Faculdade de Ciências, Universidade de Lisboa, 1749-016 Lisboa, Portugal
[3] Centro de Química e Bioquímica, Faculdade de Ciências, Universidade de Lisboa, 1749-016 Lisboa, Portugal
[4] INRS-EMT, 1650 Boulevard Lionel-Boulet, Varennes, Québec, Canada, J3X 1S2
[5] Departamento de Química e Bioquímica, Faculdade de Ciências, Universidade de Lisboa, 1749-016 Lisboa, Portugal

* **Correspondence:** Email: carmen.rangel@lneg.pt; Tel: +351210924657.

Abstract: Perovskites are important alternatives for precious metals as catalysts for bifunctional oxygen electrodes, involving oxygen evolution (OER) and reduction (ORR) reactions as is the case of regenerative fuel cells. In this work, strontium doped lanthanum ferrite $La_{1-x}Sr_xFeO_{3-\delta}$ (x = 0; 0.1; 0.2; 0.3; 0.4; 0.6 and 1.0) powders were prepared by a self-combustion route. The oxides, in the form of carbon paste electrodes, were characterised by cyclic voltammetry in alkaline solutions. Data analyses lead to the selection of $La_{0.8}Sr_{0.2}FeO_{3-\delta}$ to prepare gas diffusion electrodes (GDEs). Cyclic voltammetry and steady state polarization curves were used, respectively, to assess the electrochemical behaviour of GDEs and to obtain kinetic data for both OER and ORR. It is concluded that the oxide preparation conditions/electrode configuration determine the electrode performance. The bifunctionality of the electrodes was assessed, under galvanostatic control, using a cycling protocol within the potential domains for OER and ORR. The potential window, i.e., the total combined overpotential between OER and ORR was found to be of ≈770 mV, value which compares well with that obtained under potentiostatic control. Even though the potential window keeps constant during 140 cycles, the increase in cycling time and/or current density (≥2.5 mA cm^{-2}) led to

a gradual metallization of the GDE surface, as confirmed by Scanning Electron Microscopy and X-ray diffraction analysis.

Keywords: $La_{0.8}Sr_{0.2}FeO_{3-\delta}$; bifunctional oxygen catalyst; gas diffusion electrodes; stability

1. Introduction

Oxygen electrochemistry has been extensively studied because of its fundamental complexity as well as importance in many practical technologies and industrial processes. In particular, it is the key of several renewable energy technologies such as water electrolysis, metal-air batteries and several types of fuel cells including unitized regenerative fuel cells. One of the challenging problems in the field is to find effective electrode materials that operate alternatively as anode and cathode and catalyze the oxygen electrochemical reactions—bifunctional oxygen electrodes [1,2]. The search of a compromise between electrocatalytic activity, long-term stability and cost motivates the numerous studies on this area. Indeed, there is a lack of bifunctional oxygen catalysts, which possess high activity, reasonable electronic conductivity, low cost and stability. So far, the sluggish, strong irreversible nature of the oxygen electrochemical kinetics in conjunction with the distinct potential and conditions necessary for oxygen evolution (OER) and reduction (ORR) reactions, makes it difficult to find single bifunctional materials. Typically, the catalysts for oxygen reactions are made up of precious metals, such as Pt and Ir [3–6]. It is also well known that metals such as Pt perform quite well for ORR (but poorly for OER), while metal oxides such as RuO_2 and IrO_2 perform the other way around [7,8]. Catalyst large-scale applications are hindered by the high cost, limited supply, and poor durability for both ORR and OER [9,10,11].

The development of cost-effective catalysts, based on mixed transition metal oxides [12–19], has introduced non-precious metals as promising alternative candidates for oxygen reactions. Some perovskite-type oxides meet the mentioned requisites, namely high catalytic activity for oxygen reactions and stability in aqueous alkaline electrolytes [10–25]. However, the number of publications using perovskite materials as bifunctional catalyst is still reduced [15,17,18,19,26,27].

In 1970, Meadowcroft [20] described the use of perovskites in zinc air batteries for the first time. It was pointed out that Sr doping of $LaCoO_3$ increases both electronic conductivity and catalytic activity towards ORR in a way comparable to that of Pt. Since then, perovskite type oxides have been considered attractive electrocatalyst materials. Moreover, rare-earth and transition metals are more abundant and cheaper than platinum and other precious materials.

The catalytic activity of perovskite-type oxides (ABO_3) is quite dependent on both the transition metal element and ratio rare-earth metal/transition metal [21,22]. The tailoring of physical-chemical and catalytic properties can be fostered by partial substitution of both rare earth and transition metals. In particular, the ORR activity of perovskites correlates strongly with the transition metal cation ability to adopt different valence states, leading to the formation of redox couples at ORR potentials [2,28]. In the A-site, different lanthanides have been explored and La has demonstrated one of the best performances [29,30]. $LaNiO_3$ has been widely investigated by several groups as an oxygen catalyst [31–36]. Stability of GDEs in the OER region has been put forward in different substrates with good results when supported on Ni foam [37]. On the other hand, Mn, Co and Ni in the B-site are within the transition metals with significant impact on both ORR and OER rates while

Cr and Fe have shown high chemical and electrochemical stability in alkaline solutions [38]. Notwithstanding, the subject is complex and controversial results can be found. For instance, Manoharan and Shukla [39] found a higher catalytic activity for Co-perovskites than for Mn-perovskites, while Karlson [40] showed the opposite. The oxide synthesis method, specific surface area, support material and electrode preparation method are key factors to be considered when analysing electrodes performance.

In the past 10 years, considerable attention has been paid to perovskite materials falling within the nominal composition $La_{1-x}Sr_xMO_3$ (where M is a transition metal) as catalysts for oxygen reduction in high temperature environments, showing relatively high conductivity [41,42] and high electrocatalytic activity [43,44,45]. $La_{1-x}Sr_xFeO_{3-\delta}$ has been studied for decades as cathode and anode in high temperature fuel cells and electrolyzers, respectively [46,47]. It has been reported that the system electrocatalytic activity towards the OER increases as the fraction of oxygen vacancies and x both increase [48,49]. A similar trend was observed for compositions with $0.40 \leq x \leq 0.95$, and the highest activity in terms of exchange current density was observed for $x = 0.9$ [50]. This result was attributed to the high concentration of Fe^{4+} ions for this latter composition. Besides, $La_{1-x}Sr_xFeO_{3-\delta}$ powders with $x = 0.1$ and 0.2 used in the form of a sandwich between two nickel wire mesh were reported as bifunctional oxygen electrodes [51].

One critical issue of the development of reliable and durable perovskite bifunctional electrodes is the gradual degradation of activity at the cathode side during long-term operation, related to the formation of secondary phases besides other causes [52].

In this context strontium doped lanthanum ferrite, $La_{1-x}Sr_xFeO_{3-\delta}$ ($x = 0$; 0.1; 0.2; 0.3; 0.4; 0.6 and 1.0) powders were prepared by a self-combustion route. The oxides, in the form of carbon paste electrodes, were characterized by cyclic voltammetry in alkaline solutions. Based on this study the oxide with $x = 0.2$ was selected to prepare GDEs for further investigation of the electrocatalytic performance of strontium doped lanthanum ferrite towards OER and ORR in alkaline solutions.

The $La_{0.8}Sr_{0.2}FeO_{3-\delta}$ GDEs were characterised by cyclic voltammetry and studied as oxygen electrodes in alkaline solutions at room temperature. The cycling stability between OER and ORR was tested at different current densities. To ascertain further the electrode stability, the morphology and structure, after multiple cycles, were investigated by scanning electron microscopy coupled with energy dispersive X-ray spectrometry microanalysis (SEM/EDS) and X-ray diffraction (XRD).

2. Materials and Method

2.1. Synthesis and Characterization of Catalyst Materials

$La_{1-x}Sr_xFeO_{3-\delta}$ ($0 \leq x \leq 1$) powders were prepared by a self-combustion route, following a previously published methodology for similar compounds [53]. The starting reagents La_2O_3 (Riedel-de Haën, 99%), previously heated at 900 ℃, $FeC_2O_4 \cdot 2H_2O$ (Riedel-de Haën, 99%) and $SrCO_3$ (Aldrich, 99.9%), in the appropriate molar ratios, were dissolved in nitric acid (Sigma-Aldrich, 69%). An excess of citric acid (Sigma-Aldrich, 99.5%), relatively to the total metals ions, was added to the solution, which was gently heated until the formation of a concentrated gel. Further heating led to the gel auto-ignition and rapid combustion.

The resulting powder was heated at 600 ℃ (6 h), to remove any remaining organics, before being further calcined in air at 1000 ℃ (24 h) and 1100 ℃ (24 h), with intermediate grinding, until the desired phase was obtained, as confirmed by X-ray powder diffraction (XRD).

Structural characterization by room temperature XRD was performed using a Panalytical X'pert Pro diffractometer (θ/2θ) equipped with an X'Celerator detector and operating with monochromatized Cu-Kα radiation. The data were recorded in the 2θ range 10–80 ° with a 2θ step size of 0.017 °and a step time of 20 s.

2.2. Carbon Paste Electrodes

Carbon paste electrodes (CPEs) were prepared by hand-mixing carbon paste (BASI-CF-1010) and oxide powder in a ratio of 3:1 (w/w). This paste was then packed into the cavity of a BASI-MF-2010 electrode support. Before measurements, the electrode surface was smoothened on a piece of tracing paper in order to get a uniform, smooth and fresh surface. CPEs were employed to carry out a voltammetric study to select the most promising composition from the $La_{1-x}Sr_xFeO_{3-\delta}$ ($0 \leq x \leq 1$) series, to be used in the preparation of gas diffusion electrodes.

2.3. Gas Diffusion Electrodes

Gas diffusion electrodes were prepared on TORAY carbon paper substrates (CP), assembling a gas diffusion layer (GDL), a catalyst layer (CL) and a Nafion® layer. The gas diffusion layers were prepared from carbon black Vulcan XC-72 R powder, with a loading of 2.5 mg cm^{-2}. To fabricate the catalyst layer, an ink was prepared by suspending the material in isopropanol, and stirring in an ultrasonic bath for 10 min to thoroughly wet and disperse it. A 5% Nafion® dispersion solution (Electrochem, Inc.) was then added to the mixture. The catalyst inks were dispersed onto the gas diffusion layer with a brush, and dried at 50 ℃, until a catalyst loading of 3 mg cm^{-2} was achieved. Finally, a Nafion layer was painted over the catalyst and dried at 50 ℃ until a targeted loading of 0.7 mg cm^{-2} was reached.

The gas diffusion electrode samples contact to an electrical wire was made using a conducting silver epoxide. The electrodes were then mounted in a glass tube, which was sealed with epoxy resin.

Electrode morphology and elemental composition, before and after cycling, were assessed using a scanning electron microscope Philips XL 30 FEG model, with a field emission electron source, operated with acceleration voltage of 15 kV, and coupled with an energy dispersive X-ray microanalysis spectrometer. The Si (Li) detector is equipped with a 3 mm super ultrathin window (SUTW) allowing detection and quantification of elements with low characteristic X-ray, such as oxygen.

2.4. Electrochemical Studies

A conventional three-electrode glass cell was used. The measurements were carried out at room temperature, using Hg/HgO/1 M KOH (98 mV vs. SHE) electrode as reference and a graphite bar as counter electrode. A potassium hydroxide 1 M solution was prepared using Millipore Milli-Q ultrapure water.

The experiments were performed using a computer controlled Gamry 600 potentiostat/galvanostat.

Oxygen evolution and reduction reactions, on both CPEs and GDEs, were studied under oxygen equilibrium conditions. Cyclic voltammograms were recorded in N_2-saturated 1 M KOH solutions at a sweep rate (v) of 10 mV s^{-1}. Polarization curves were obtained in the potential range where the oxygen evolution (730 to 400 mV) and reduction (250 to −350 mV) occur, under N_2 or O_2-saturated 1 M KOH, at v = 0.2 mV s^{-1}.

GDE cycling was carried out under galvanostatic control in 1 M KOH solutions for a sustained period of time of 300 s in each region (OER and ORR) during the performance of 140 full cycles, using current densities of 0.44, 1.11 and 2.45 mA cm^{-2}.

3. Results and Discussion

3.1. Choice of the Oxide Composition to Integrate the GDE

Figure 1 presents the current densities (c.ds.) for OER and ORR for $La_{1-x}Sr_xFeO_{3-\delta}$ (x = 0; 0.1; 0.2; 0.3; 0.4; 0.6 and 1.0) CPEs, obtained from voltammetric curves at E = 650 and −200 mV vs Hg/HgO, respectively.

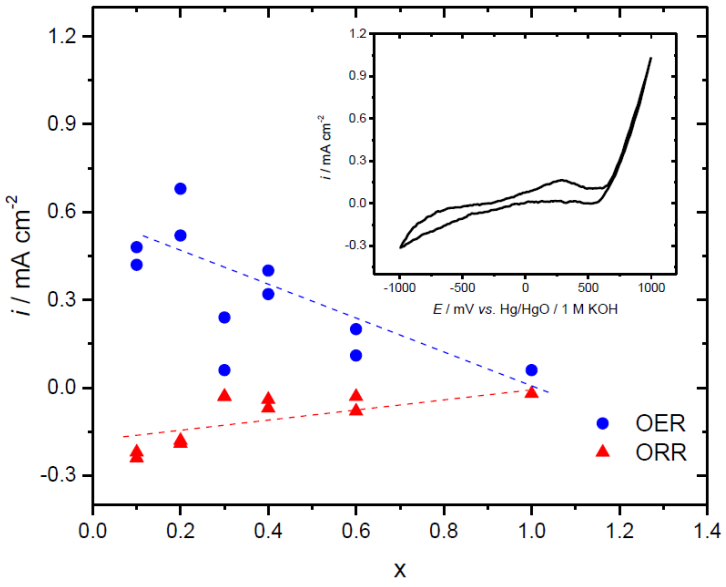

Figure 1. Current densities for OER and ORR at E = 650 and −200 mV vs Hg/HgO, respectively, obtained from voltammetric curves on $La_{1-x}Sr_xFeO_{3-\delta}$ (x = 0; 0.1; 0.2; 0.3; 0.4; 0.6 and 1.0) oxides in the form of carbon paste electrodes in 1 M KOH at v = 10 mV s^{-1}. Inset presents a cyclic voltammogram in 1 M KOH for the nominal composition x = 0.2 at v = 10 mV s^{-1}.

Considering that the amount of carbon is the same for all the electrodes, the results clearly indicate that both OER and ORR c.ds. decrease with increasing of the Sr amount in the samples. These results disagree with those reported by other authors [48,49,50], that observed an increase on the electrocatalytic activity for OER with increasing x. This disagreement likely results from differences in the materials synthesis conditions, that most probably affect the Fe^{3+}/Fe^{4+} ratio and the amount of oxygen vacancies in the bulk [50]. Figure 1 also shows that among the studied samples the

ones with x = 0.1 and 0.2 exhibit the highest c.ds. for both OER and OER. Based on these preliminary results and knowing that the conductivity of the x = 0.2 composition is higher than for x = 0.1, the sample with nominal composition $La_{0.8}Sr_{0.2}FeO_{3-\delta}$ was selected to prepare GDEs and investigate in detail its bifunctionality for oxygen reactions [50,54].

A cyclic voltammogram (CV) for the nominal composition x = 0.2 at v = 10 mV s^{-1} is displayed in the inset of Figure 1. For this composition, voltammetric curves obtained in the pseudo-capacitive potential range showed an almost rectangular profile, indicating a very limited ohmic drop (not shown). This result also supports the choice of the sample with nominal composition $La_{0.8}Sr_{0.2}FeO_{3-\delta}$.

3.2. Structural Characterization

The XRD pattern of $La_{0.8}Sr_{0.2}FeO_{3-\delta}$ is presented in Figure 2 together with that of $LaFeO_3$, prepared using the same methodology. The comparison between the two patterns shows that some minor diffraction peaks (namely around 2θ = 25.3, 34.2 and 47.6 °) are absent for the x = 0.2 data. Based on these differences, and considering other results obtained for similar materials, which indicated three different crystallographic regions (orthorhombic, rhombohedral and cubic) depending on x value [53,55], both orthorhombic and rhombohedral structures were tested. The results clearly indicated that, while $LaFeO_3$ present an orthorhombic structure, as previously referred [53], the $La_{0.8}Sr_{0.2}FeO_{3-\delta}$ compound is better described by a rhombohedral structure ($R\bar{3}c$). Nevertheless, the calculated cell parameters of $La_{0.8}Sr_{0.2}FeO_{3-\delta}$ obtained in the present work, a = 5.523 Å and c = 13.435 Å, show that the rhombohedral distortion ($a\sqrt{6}/c$) is very small (1.007).

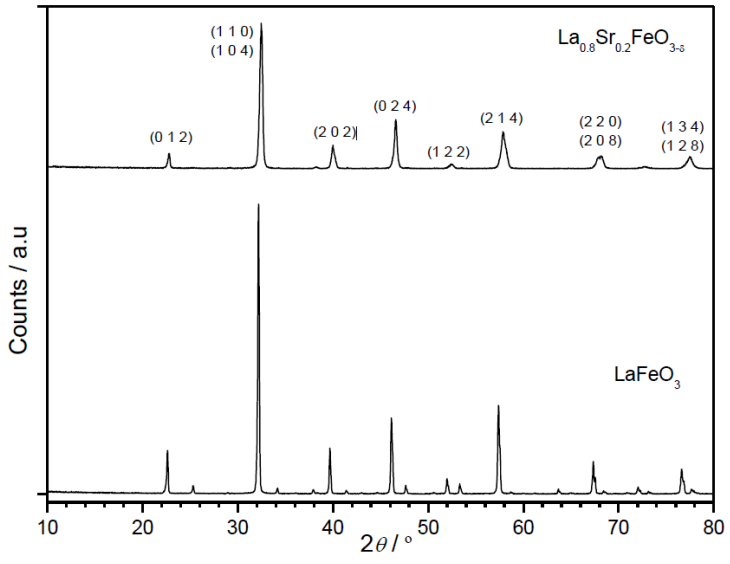

Figure 2. X-ray diffraction patterns for $LaFeO_3$ and $La_{0.8}Sr_{0.2}FeO_{3-\delta}$ powder samples.

3.3. Cyclic Voltammetry

A representative stabilized cyclic voltammogram for $La_{0.8}Sr_{0.2}FeO_{3-\delta}$ gas diffusion oxide electrode (CP/GDL/$La_{0.8}Sr_{0.2}FeO_{3-\delta}$), recorded after 10 cycles, in N_2-saturated 1 M KOH is

presented in Figure 3. For comparison purposes a voltammogram for a CP substrate coated with a Nafion® layer (CP/GDL) and oxide free, recorded under the same conditions is also presented.

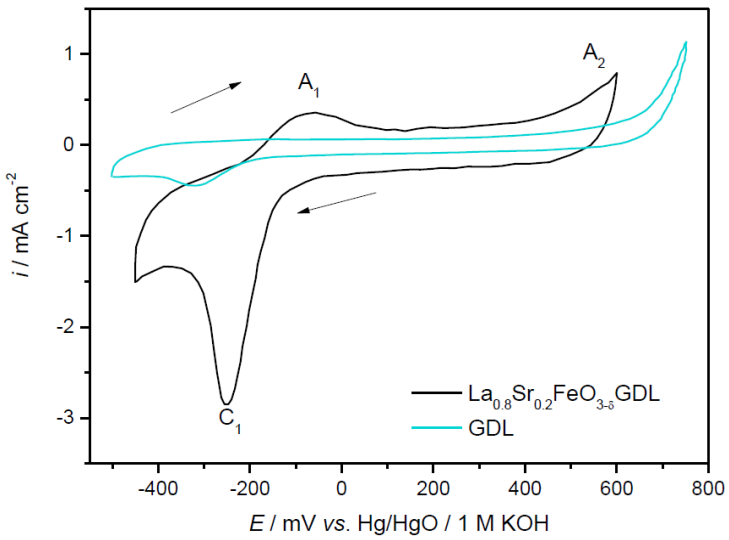

Figure 3. Cyclic voltammograms recorded for CP/GDL/$La_{0.8}Sr_{0.2}FeO_{3-\delta}$ oxide coating and CP substrate coated with a Nafion® layer, in N_2-saturated 1 M KOH at v = 10 mV s^{-1}. Current normalized for the electrodes' geometric area.

For the CP/GDL/$La_{0.8}Sr_{0.2}FeO_{3-\delta}$ electrode, a broad peak (A_1) centered at ≈−100 mV and an increase of current for E > 400 mV (A_2) are observed on the anodic sweep. On the reverse sweep, only one corresponding large peak appears at ≈−250 mV (C_1). Peak C_1 is assumed to involve the simultaneous reduction of the oxide (probably Fe^{4+} to Fe^{3+}) along with the reduction of the oxygen produced in the rising current A_2 [48]. In accordance, the broad peak A_1 is attributed to the oxide re-oxidation. This assignment is consistent with the absence of peak A_1 on the CV recorded for the CP/GDL electrode. On the other hand, contributions from the oxidation of both oxide and carbon to the rising current A_2 cannot be excluded [37,56,57]. According to Augustin et al. [58] the oxidation behavior of perovskite oxides are predominantly governed by the oxygen evolution mechanism. The voltammetric profiles also show a significant contribution from the oxide to the pseudo-capacitive current density and consequently to an increase of the electrochemical surface area. Indeed a value of 233 ± 33 was obtained for the electrodes roughness factor, calculated from cyclic voltammograms recorded in the double layer region at various sweep rates, in accordance with an approach well established in the literature [59]. Values of the same order of magnitude were obtained, in our laboratory, when using $LaNiO_3$ supported on CP/GDL [37].

The data in Figure 3 also show that CP/GDL/$La_{0.8}Sr_{0.2}FeO_{3-\delta}$ electrode, for both ORR and OER, initiates at lower potentials and with higher current densities when compared with CP/GDL electrode. The onset potential for OER is more positive (≈100 mV) for the CP/GDL electrode than for CP/GDL/$La_{0.8}Sr_{0.2}FeO_{3-\delta}$ electrode. For the ORR, the onset is less negative (≈100 mV) than that of CP/GDL electrode and presents smaller current densities. These results indicate that carbon contribution, for both ORR and OER, can be neglected under the tested conditions, although several studies refer the contribution of carbon into the ORR and OER kinetics on CP/GDL/perovskite oxide electrodes [56,60–63].

3.4. Oxygen Reactions

Figure 4 shows polarization curves for CP/GDL/$La_{0.8}Sr_{0.2}FeO_{3-\delta}$ electrodes obtained in N_2 or O_2-saturated 1 M KOH solution, in the potential range where the OER (a) and ORR (b) take place. The insets show the respective Tafel plots corrected for the uncompensated ohmic drop. Meaningful current densities for OER could be measured for potentials higher than 600 mV. Since the equilibrium potential of the oxygen electrode in basic solution is +300 mV vs. Hg/HgO/1 M KOH, a minimum overpotential of ≈300 mV is needed for oxygen evolution to occur. From the Tafel plot, apparent exchange current density (i_0) of (5.3 ± 0.4) × 10^{-8} A cm^{-2} and slope of 72 ± 5 mV were estimated. Values between 55 and 58 mV were published by Suresh et al. [51] for $La_{0.8}Sr_{0.2}FeO_{3-\delta}$ oxides prepared by a solution method and sandwiched between two Ni wire mesh electrodes. The discrepancy on Tafel slopes can be due to the use of different electrode configuration and/or to the oxide preparation methods, which may influence the electrocatalytic activity of the electrodes [64]. Indeed differences in the oxides synthesis conditions could lead to variations on the Fe^{3+}/Fe^{4+} ratio and oxygen vacancies that will affect the OER mechanism [49,50]. Wattiaux et al. [50] obtained Tafel slopes between 75 and 96 mV for $La_{1-x}Sr_xFeO_{3-\delta}$ ($0.40 \leq x \leq 0.95$) pelleted oxide electrodes and i_0 ranging from 4.4 × 10^{-13} to 2.0 × 10^{-11} A cm^{-2}, for OER in the low potential region. A comparison between these results with those found in this work is not straight forward, since the degree of substitution affects the electrocatalytic activity of the $La_{1-x}Sr_xFeO_{3-\delta}$ system towards the OER in addition to oxide preparation method and electrode configuration, as already stated.

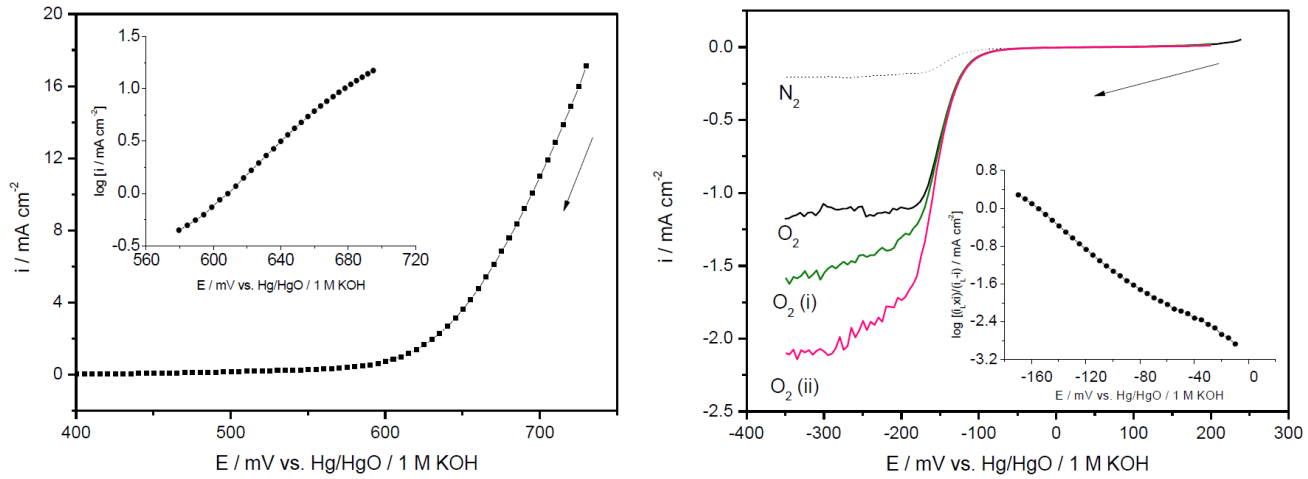

Figure 4. Anodic (a) and cathodic (b) polarization curves for CP/GDL/$La_{0.8}Sr_{0.2}FeO_{3-\delta}$ in 1 M KOH. The cathodic curves were obtained under N_2 or O_2 atmospheres without stirring and with i) 300 and ii) 500 rpm. Insets show the respective Tafel plots corrected for ohmic drop. Current is normalized for the electrode's geometric area.

Figure 4b displays a family of linear voltammograms for CP/GDL/$La_{0.8}Sr_{0.2}FeO_{3-\delta}$ electrodes in the ORR potential range, with 300 and 500 rpm (i, ii) and without stirring in O_2-saturated 1 M KOH solution. A linear voltammogram in a N_2-saturated solution is also presented. It is noticed a small reduction current at ca. −150 mV, followed by a plateau which are related with the oxide reduction

(probably Fe^{4+} to Fe^{3+}) already observed in the cyclic voltammograms. In contrast, higher current densities are observed in the O_2-saturated solutions as expected. In this case, no major variation of current density with stirring is observed between ≈−50 and −140 mV vs. Hg/HgO/1 M KOH consistent with charge transfer kinetics control followed by a mixed control region. At higher negative potentials, a well-defined limiting current is recorded, dependent on stirring rate.

For the ORR Tafel analysis, the data points were chosen from the kinetically controlled region and corrected for mass-transport effects by calculating the parameter $i_L i/(i_L - i)$, where i is the current density at any potential and i_L the voltammetric limiting current density [65]. The Tafel plots show one well-defined region (correlation coefficients better than 0.98) extending over two orders of magnitude in current density. A Tafel slope of 45 ± 3 mV and $i_0 = (3.7 \pm 0.4) \times 10^{-11}$ mA cm^{-2} were estimated. It is worthwhile to state that the obtained Tafel slope for ORR is lower than the values reported by Suresh et al. (115–130 mV) [51]. This could be due, as referred above, to different oxide preparation methods and/or electrode configuration. In what concerns the i_0 values, no data were available in the literature, for this composition.

As a final remark, it can be said that, the oxide preparation conditions and electrode configuration used in this work promote a better performance of the CP/GDL/$La_{0.8}Sr_{0.2}FeO_{3-\delta}$ electrodes.

The OER/ORR potential window is currently used as a tool to compare the bifuntional activity of catalyst materials. In this study, it was made the quantification of the $La_{0.8}Sr_{0.2}FeO_{3-\delta}$ GDE electrochemical window associated to the potential difference between the OER and ORR measured at 10 mA cm^{-2} and −1 mA cm^{-2}, respectively (Figure 5). A value of 850 mV was obtained that is comparable to those recently reported for bifunctional catalysts such as $La_{0.6}Sr_{0.4}Fe_{0.8}Co_{0.2}O_3$/carbon composite (894 mV) [66] and $Ba_{0.5}Sr_{0.5}Co_{0.8}Fe_{0.2}O_{3-\delta}$ on N-doped mesoporous carbon (840 mV) [67] and lower than the one obtained by Zhu et al. [68] for $La_{0.95}FeO_{3-\delta}$ perovskite (1090 mV). This is a promising result. Constant current density experiments, more appropriate for the assessment of the electrochemical window, were also implemented. Results of cycling between OER and ORR domains are presented below.

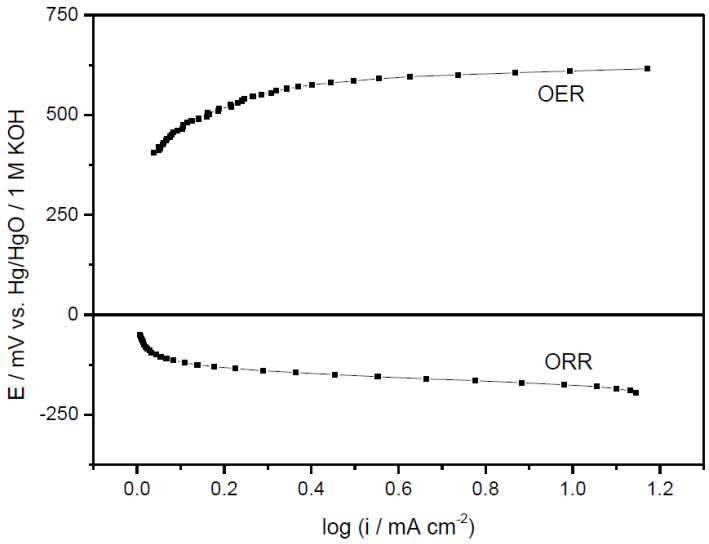

Figure 5. Anodic and cathodic polarization curves for CP/GDL/$La_{0.8}Sr_{0.2}FeO_{3-\delta}$ in 1 M KOH at v = 0.2 mV s^{-1}. Current is normalized for the electrodes' geometric area.

3.5. Bifunctionality

Constant current density cycling experiments were carried out in order to assess electroactivity of the CP/GDL/$La_{0.8}Sr_{0.2}FeO_{3-\delta}$ electrodes during sustained periods of time (300 s) at oxygen reduction and evolution. The electrodes were cycled between OER and ORR using c.ds. of 0.44, 1.11 and 2.45 mA cm^{-2}. For the lowest current density, the first 3 full cycles are displayed in Figure 6. The electrodes exhibited a stable potential for both OER and ORR with values around 600 and −175 mV vs. Hg/HgO/1 M KOH, respectively. Similar patterns were obtained for the other current densities tested.

These potential values are lower than those reported by Alegre et al. for $La_{0.6}Sr_{0.4}Fe_{0.8}Co_{0.2}O_3$/carbon composite, although their experiments were performed at a much higher applied current density of 80 mA cm^{-2} [69].

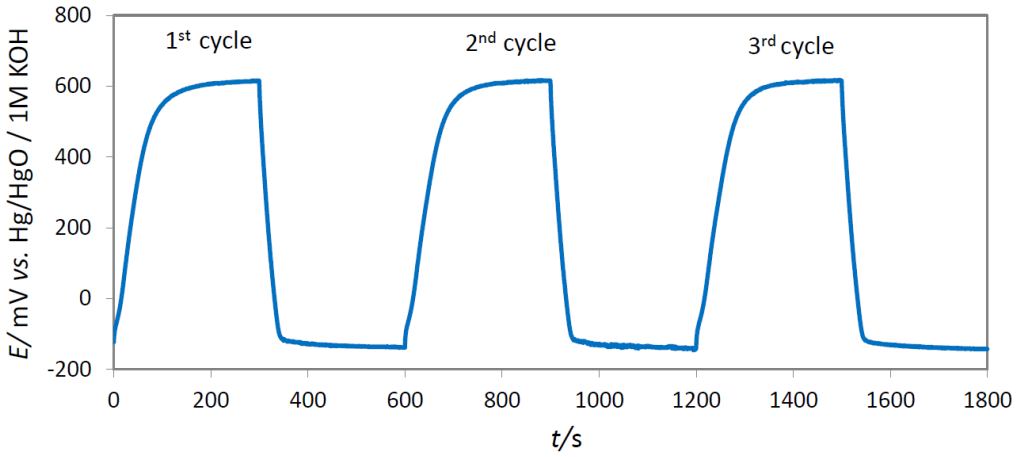

Figure 6. Potential vs. time response of CP/GDL/$La_{0.8}Sr_{0.2}FeO_{3-\delta}$ during cycling between OER and ORR at 0.44 mA cm^{-2}, at room temperature. First 3 cycles.

For additional evaluation of the electrodes performance, a set of selected cycles up to the 140th, are presented in Figures 7a–c), for the three tested current densities. The results demonstrate that the electrode is stable regarding repeated cycling between OER and ORR conditions, for current densities of 0.44 and 1.11 mA cm^{-2}, with the potential quickly reaching a well-defined plateau value in both cases. Moreover, when switching from anodic to cathodic current, i.e., from OER to ORR, the transition in the potential vs. time curves is very fast and linear. When reversing the current to OER, a more sluggish response is observed with an initial rise time of ≈100 s, which decreases with cycling. This behaviour is associated with perovskite surface oxidation [50]. Even though, this value is much lower than that exhibited by other bifunctional compounds reported in the literature, which transition from ORR to OER expands to times—between 10 and 20 minutes [70]. After 140 cycles the potentials for the OER and ORR on-set are separated by ≈770 mV, as shown in Figures 7a and 7b. The ΔE values are smaller than those obtained for noble metal catalysts such as Pt (1160 mV) and Ir (920 mV) when current densities of 3 and 10 mA cm^{-2} were applied for ORR and OER respectively [71].

For c.d. of 2.45 mA cm^{-2} the electrode demonstrates a fair stability for the OER with negligible potential changes and anodic profiles similar to the ones observed for the lower current densities

(Figure 7c). In contrast a poor stability is observed in the cathodic region for cycle number >50 with the potential rising gradually over the following cycles. It is interesting to note that, when reversing the current to OER, after cycle number 80, a decrease on the rise time is observed with cycling, indicating a complete oxidation of the perovskite surface.

A comparison of the OER and ORR potential values for selected number of cycles is presented in Figure 7d. As expected, the OER potential does not vary with current density indicating a minimal loss of catalytic capability. With respect to the ORR a potential increase is observed when using 2.45 mA cm^{-2}, especially from the 50^{th} cycle onwards, indicating instability/degradation of the electrode.

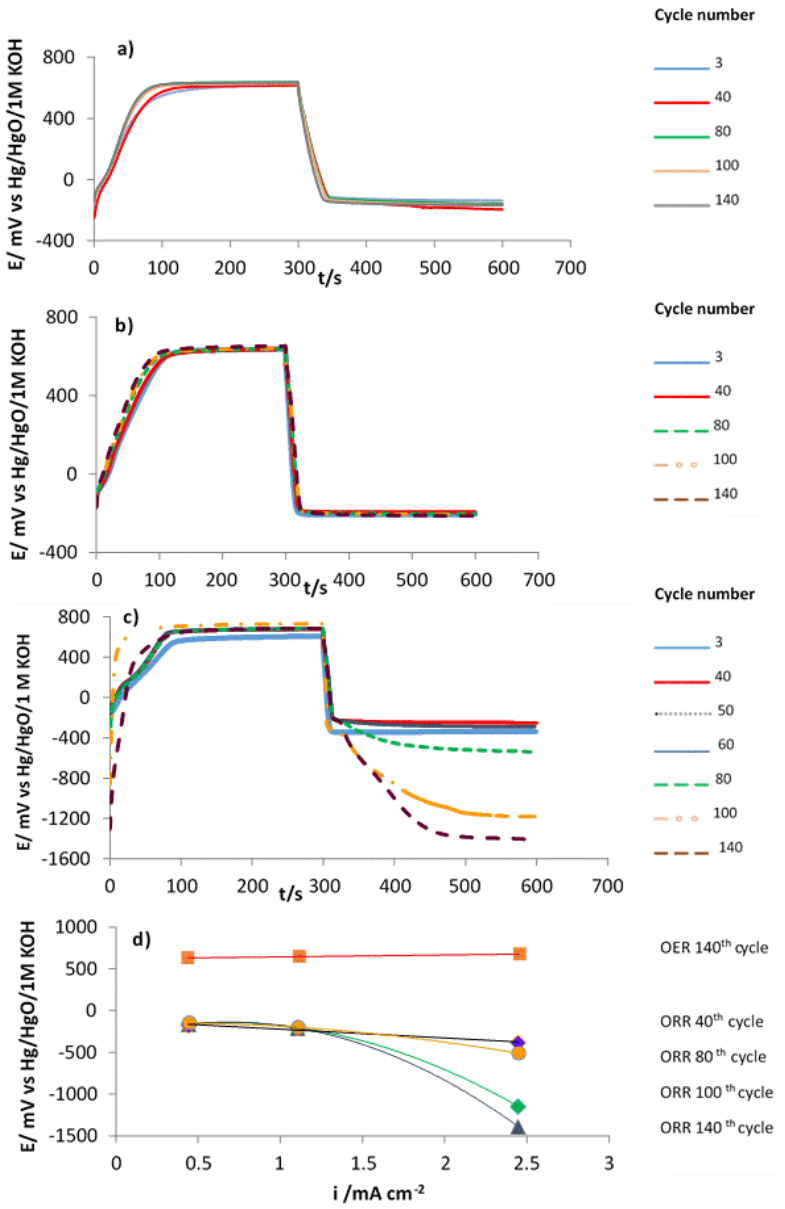

Figure 7. Potential vs. time response of CP/GDL/$La_{0.8}Sr_{0.2}FeO_{3-\delta}$ during cycling between OER and ORR, for selected cycles up to the 140^{th} cycle at (a) 0.44 (b) 1.11 and (c) 2.45 mA cm^{-2}. Plot of the potential values for OER and ORR vs. current densities for selected cycles up to 140 (d).

3.6. Stability

To further confirm the stability of the CP/GDL/$La_{0.8}Sr_{0.2}FeO_{3-\delta}$ electrodes, the morphology and structure after cycling were investigated by SEM/EDS and XRD.

Figure 8 shows representative SEM imagesof the electrodes surface before (a) and after cycling under galvanostatic control at 0.44 (b) 1.11 (c) and 2.45 mA cm^{-2} (d). Before cycling the electrode surface exhibits a porous and granular morphology. Individual particles are not visible and the aggregates have irregular shapes. After cyclicing at 0.44 mA cm^{-2} the surface morphology appears without apparent modification. For the other cycling conditions, the surface morphology clearly changes. The images indicate the presence of a new and more compact phase, suggesting surface mettalisation.

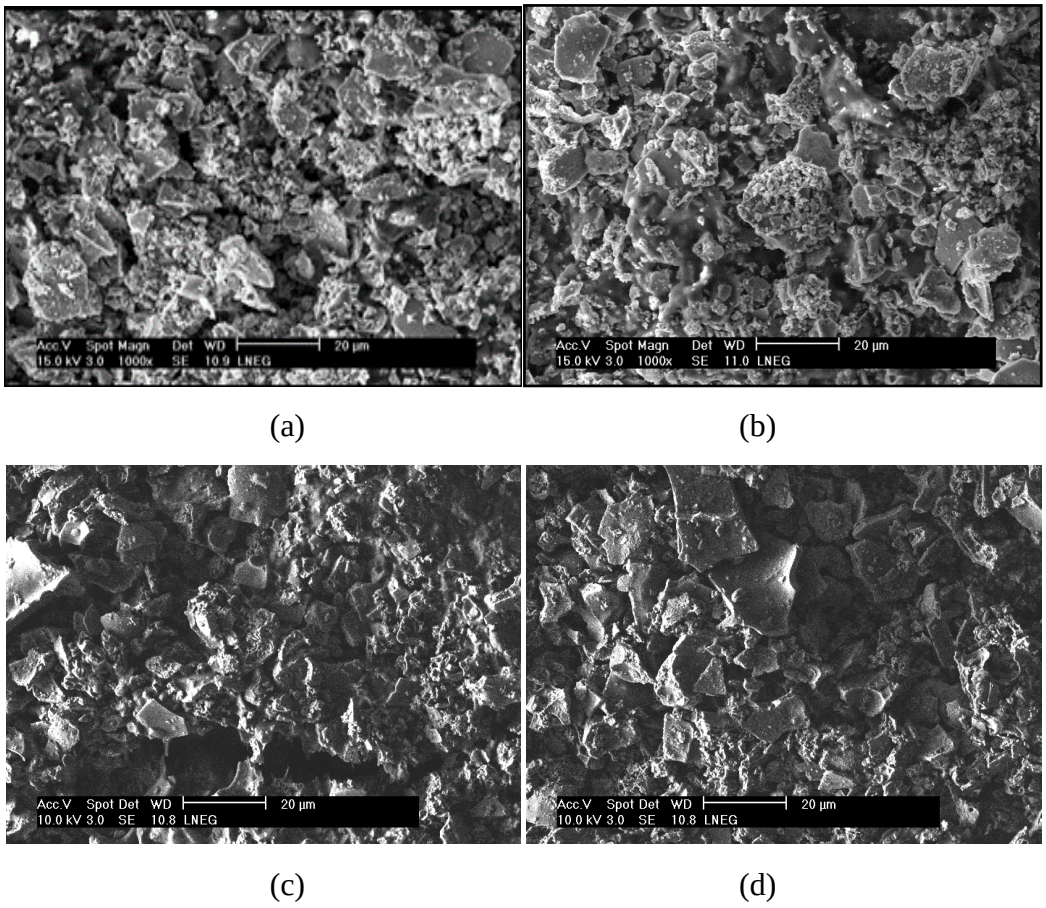

Figure 8. Representative SEM images of the electrodes surface before (a) and after cycling under galvanostatic control at 0.44 (b) 1.11 (c) and 2.45 mA cm^{-2} (d).

The CP/GDL electrode was also examined by SEM in cross section, after 140 cycles under galvanostatic control at 0.44 mA cm^{-2}, as shown in Figure 9. In this image, the catalytic layer, the GDL and the carbon fibers of the CP support are clearly visible, as supported by EDS analysis. In fact, the qualitative EDS analysis was conducted in the different layers showing the associated elemental compositions: region 1 with the presence of La, Sr, Fe, and O from the catalyst and elements such as S, F, and C, indicate that the electrode has kept integrity regarding the additives

used in the preparation of the catalyst ink. Also shown in Figure 9 are the EDS spectra corresponding to typical elements of the diffusion layer and carbon support, exhibited for regions identified in the SEM micrograph as 2 and 3 respectively. The catalytic layer after cycling did not show meaningful modifications regarding initial composition.

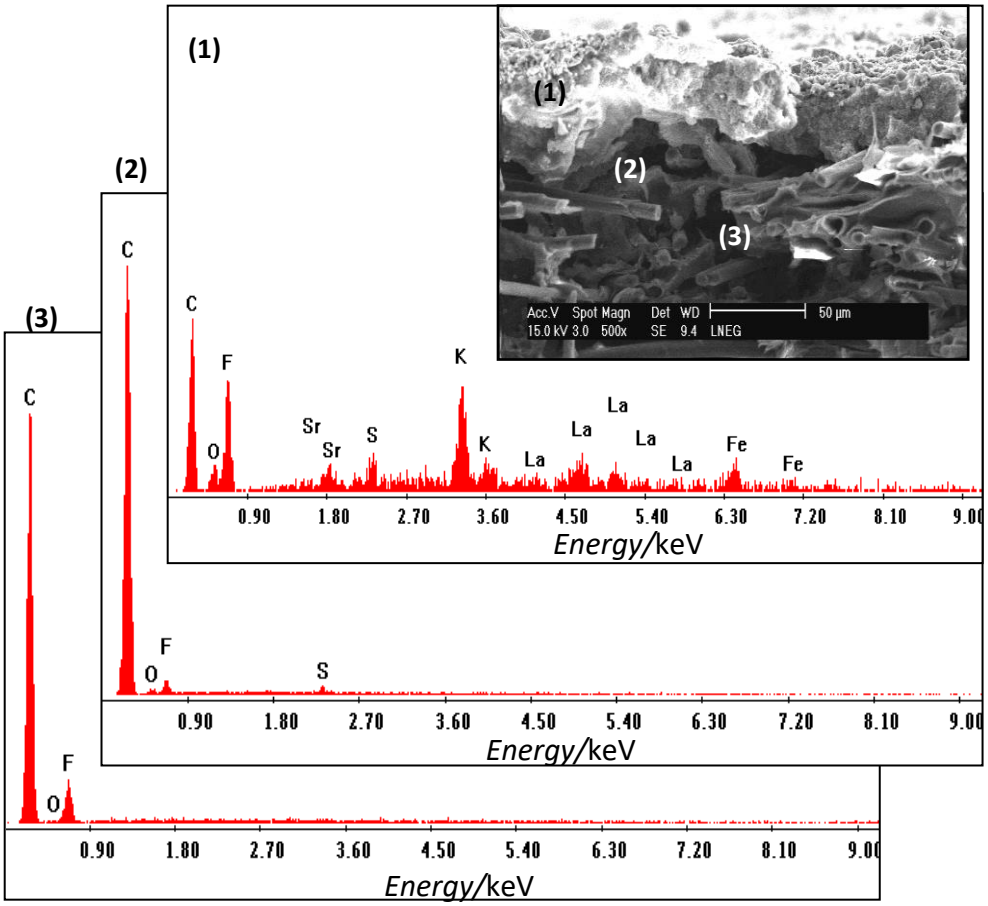

Figure 9. Cross section SEM image of the CP/GDL/$La_{0.8}Sr_{0.2}FeO_{3-\delta}$, after cycling at 0.44 mA cm^{-2}, presenting 3 different regions. EDS spectra showing elemental composition of the catalyst layer (1), gas diffusion layer (2) and CP support (3).

The XRD patterns for the CP/GDL/$La_{0.8}Sr_{0.2}FeO_{3-\delta}$ electrodes before and after cycling are presented in Figure 10. For comparison, the pattern of the powder before incorporation (a) is included. A comparison between the X-ray diffraction patterns of the electrodes before and after cycling showed that all the electrodes maintain the perovskite-type structure. The results also demonstrate that, for the lowest c.d., the electrodes are stable regarding repeated cycling between OER and ORR. However, for higher c.d. (1.11 and 2.45 mA cm^{-2}), the diffractograms indicate the formation of additional peaks, identified as due to the presence of metallic iron (α-Fe).

For the lowest c.d., XRD patterns of the new and cycled electrode are identical and all peaks were identified as the perovskite-type phase, $La_{0.8}Sr_{0.2}FeO_{3-\delta}$, and carbon from the CP support. No significant changes were observed for the electrodes after cycling in agreement with electrochemical data presented in Figure 7a.

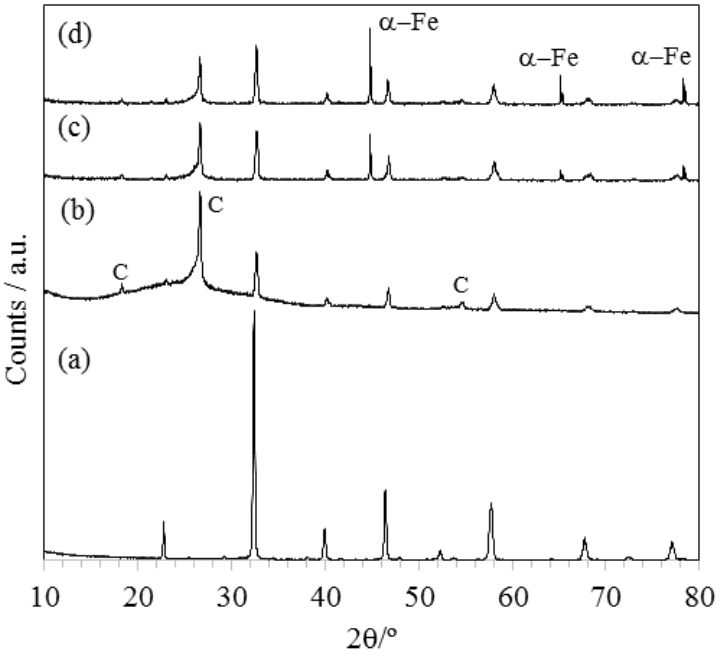

Figure 10. X-ray diffraction patterns of CP/GDL/$La_{0.8}Sr_{0.2}FeO_{3-\delta}$ after 140 cycles at (b) 0.44 mA cm^{-2} (c) 1.11 mA cm^{-2} and (d) 2.25 mA cm^{-2} between OER and ORR. Pattern of the powder before incorporation (a) is included for comparison.

According to Bronoel et al. [48] $La_{1-x}Sr_xFeO_{3-\delta}$ compounds undergo reduction along with the reduction of oxygen. The results suggest that for higher current densities the reduction of the oxide may be predominant in the cathodic region. The formation of metallic α-Fe substantially degrades the electrochemical activity and stability of the CP/GDL/$La_{0.8}Sr_{0.2}FeO_{3-\delta}$ electrodes for the ORR.

In summary, regarding the ORR (Figures 7b and 7c), an increase in applied current density lead to a gradual decay in the potential values associated to the perovskite degradation as confirmed by SEM/EDS and X-ray diffraction.

One possible explanation for the oxide degradation is that during the cathodic semi-cycle, Fe^{3+} ions in the perovskite lattice tend to be reduced to $HFeO_2^-$ water soluble species [72], which are further reduced leading to the formation of metallic iron [73].

On the basis of this hypothesis, the degradation of the perovskite phase and the formation of α-Fe may be described by the following reduction reactions:

$$Fe^{3+} + 3OH^- + e^- \rightarrow HFeO_2^- + H_2O \quad (1)$$

$$HFeO_2^- + H_2O + 2e^- \rightarrow Fe + 3OH^- \quad (2)$$

According to Karlson and Lindstrom [74] the perovskite degradation during the cathodic semi-cycle is associated with the high anodic potentials reached during the oxygen evolution reaction. These authors observed that impregnating the perovskite oxide $La_{0.5}Sr_{0.5}CoO_3$ with nickel was effective in lowering the OER potential, avoiding the high anodic potentials that lead to dissolution of the electrocatalyst.

4. Conclusions

Gas diffusion electrodes CP/GDL/$La_{0.8}Sr_{0.2}FeO_{3-\delta}$ were assembled from own synthesized perovskite and tested as oxygen bifunctional electrodes in alkaline medium. By comparing the kinetic data obtained for the OER and ORR with those referred in the literature for the same oxide composition it was concluded that the oxide preparation conditions/electrode configuration determine the electrode performance. SEM and XRD analysis indicated no apparent degradation of the catalyst layer, after 140 cycles under galvanostatic control for low current densities, namely 0.44 mA cm^{-2}, exhibiting an electrochemical window of ≈770 mV. On the other hand a clear partial decomposition occurs during cycling at 2.45 mA cm^{-2} with a slow metallization of the electrode, which limits the useful electrode life to c.d. <1.11 mA cm^{-2}. These observations suggest that, for high current densities, the oxide reduction may be predominant in the cathodic region, caused by the anodic oxide dissolution. In order to overcome this problem it is envisaged further studies of the prepared and characterized $La_{0.8}Sr_{0.2}FeO_{3-\delta}$ perovskite oxide impregnated with Ni in the form of GDEs. Also considered is the progressive substitution of Fe by Ni in the perovskite oxide. Optimization of these options may bring about improved stability and enhance redox efficiency.

Acknowledgments

Partial financing of the work under contract PTDC/CTM/102545/2008 and UID/MULTI/00612/2013 is acknowledged. C.O. Soares acknowledges a grant under the same contract.

Conflict of Interest

All authors declare no conflicts of interest in this paper.

References

1. Lee J, Jeonga B, Ocona JD (2013) Oxygen electrocatalysis in chemical energy conversion and storage technologies. *Curr Appl Phys* 13: 309–321.
2. Jorissen L (2006) Bifunctional oxygen/air electrodes. *J Power Sources* 155: 23–32.
3. Kong FD, Zhang S, Yin GP, et al. (2012) Preparation of $Pt/Ir_x(IrO_2)_{10-x}$ bifunctional oxygen catalyst for unitized regenerative fuel cell. *J Power Sources* 210: 321–326.
4. Jung HY, Park S, Popov BN (2009) Electrochemical studies of an unsupported PtIr electrocatalyst as a bifunctional oxygen electrode in a unitized regenerative fuel cell. *J Power Sources* 191: 357–361.
5. Wang B (2005) Recent development of non-platinum catalysts for oxygen reduction reaction. *J Power Sources* 152: 1–15.
6. Pettersson J, Ramsey B, Harrison D (2006) A review of the latest developments in electrodes for unitised regenerative polymer electrolyte fuel cells. *J Power Sources* 157: 28–34.
7. Park S, Shao YY, Liu J, et al. (2012) Oxygen electrocatalysts for water electrolyzers and reversible fuel cells: status and perspective. *Energ Environ Sci* 5: 9331–9344.

8. Cheng FY, Chen J (2012) Metal–air batteries: from oxygen reduction electrochemistry to cathode catalysts. *Chem Soc Rev* 41: 2172–2192.
9. Chen ZW, Higgins D, Yu AP, et al. (2011) A review on non-precious metal electrocatalysts for PEM fuel cells. *Energ Environ Sci* 4: 3167–3192.
10. Shao YY, Park S, Xiao J, et al. (2012) Electrocatalysts for nonaqueous lithium–air batteries: status, challenges, and perspective. *ACS Catal* 2: 844–857.
11. Othman R, Dicks AL, Zhu ZH (2012) Non precious metal catalysts for the PEM fuel cell cathode. *Int J Hydrogen Energ* 37: 357–372.
12. Prakash J, Tryk D, Yeager E (1990) Electrocatalysis for oxygen electrodes in fuel cells and water electrolyzers for space applications. *J Power Sources* 29: 413–422.
13. Rios E, Gautier JL, Poillerat G, et al. (1998) Mixed valency spinel oxides of transition metals and electrocatalysis: case of the $Mn_xCo_{3-x}O_4$ system. *Electrochim Acta* 44: 1491–1497.
14. Nikolova V, Iliev P, Petrov K, et al. (2008) Electrocatalysts for bifunctional oxygen/air electrodes. *J Power Sources* 185: 727–733.
15. Chang YM, Wu PW, Wu CY, et al. (2009) Synthesis of $La_{0.6}Ca_{0.4}Co_{0.8}IrO_3$ perovskite for bi-functional catalysis in an alkaline electrolyte. *J Power Sources* 189: 1003–1007.
16. Tulloch J, Donne SW (2009) Activity of perovskite $La_{1-x}Sr_xMnO_3$ catalysts towards oxygen reduction in alkaline electrolytes. *J Power Sources* 188: 359–366.
17. Zhuang S, Huang K, Huang C, et al. (2011) Preparation of silver-modified $La_{0.6}Ca_{0.4}CoO_3$ binary electrocatalyst for bi-functional air electrodes in alkaline medium. *J Power Sources* 196: 4019–4025.
18. Wu X, Scott K (2012) A non-precious metal bifunctional oxygen electrode for alkaline anion exchange membrane cells. *J Power Sources* 206: 14–19.
19. Jin C, Cao X, Zhang L, et al. (2013) Preparation and electrochemical properties of urchin-like $La_{0.8}Sr_{0.2}MnO_3$ perovskite oxide as bifunctional catalyst for oxygen reduction and oxygen evolution reaction. *J Power Sources* 241: 225–230.
20. Meadowcroft DB (1970) Low-cost oxygen electrode material. *Nature* 226: 847–848.
21. Tejuca LG, Fierro JLG, Tascon JMD (1989) Structure and reactivity of perovskite-type oxides. *Adv Catal* 36: 237–328.
22. Boivin JC, Mairesse G (1998) Recent material developments in fast oxide ion conductors. *Chem Mater* 10: 2870–2888.
23. White JH, Sammells AF (1993) Perovskite anode electrocatalysis for direct methanol fuel cells. *J Electrochem Soc* 140: 2167–2177.
24. Yu HC, Fung KZ, Guo TC, et al. (2004) Syntheses of perovskite oxides nanoparticles $La_{1-x}Sr_xMO_{3-\delta}$ (M = Co and Cu) as anode electrocatalyst for direct methanol fuel cell. *Electrochim Acta* 50: 811–816.
25. Velraj S, Zhu JH (2013) $Sm_{0.5}Sr_{0.5}CoO_{3-\delta}$—A new bi-functional catalyst for rechargeable metal-air battery applications. *J Power Sources* 227: 48–52.
26. Wang L, Ara M, Wadumesthrige K, et al. (2013) Graphene nanosheet supported bifunctional catalyst for high cycle life Li-air batteries. *J Power Sources* 234: 8–15.
27. Noroozifar M, Khorasani-Motlagh M, Ekrami-Kakhki MS, et al. (2014) Enhanced electrocatalytic properties of Pt–chitosan nanocomposite for direct methanol fuel cell by $LaFeO_3$ and carbon nanotube. *J Power Sources* 248: 130–139.

28. Peňa MA, Fierro JLG (2001) Chemical structures and performance of perovskite oxides. *Chem Rev* 101: 1981–2018.
29. Armstrong NH, Duncana KL, Wachsman ED (2013) Effect of A and B-site cations on surface exchange coefficient for ABO_3 perovskite materials. *Phys Chem Chem Phys* 15: 2298–2308.
30. Marti PE (1994) Influence of the A-site cation in $AMnO_{3+x}$ and $AFeO_{3+x}$ (A = La, Pr, Nd and Gd) perovskite-type oxides on the catalytic activity for methane combustion. *Catal Lett* 26: 71–84.
31. Swette L, Kackley N, McCatty SA (1991) Oxygen electrodes for rechargeable alkaline fuel cells. III. *J Power Sources* 36: 323–339.
32. Kannan AM, Shukla AK, Sathyanarayana SJ (1989) Oxide-based bifunctional oxygen electrode for rechargeable metal/air batteries. *J Power Sources* 25: 141–150.
33. Kannan AM, Shukla AK (1990) Rechargeable iron/air cells employing bifunctional oxygen electrodes of oxide pyrochlores. *J Power Sources* 35: 113–121.
34. Swette L, Kackley N (1990) Oxygen electrodes for rechargeable alkaline fuel cells – II. *J Power Sources* 29: 423–436.
35. Soares CO, Carvalho MD, Jorge MEM, et al. (2012) High Surface area $LaNiO_3$ electrodes for oxygen electrocatalysis in alkaline media. *J Appl Electrochem* 42: 325–332.
36. Soares CO, Silva RA, Carvalho MD, et al. (2013) Oxide loading effect on the electrochemical performance of $LaNiO_3$ coatings in alkaline media. *Electrochim Acta* 89: 106–113.
37. Silva RA, Soares CO, Carvalho MD, et al. (2014) Stability of $LaNiO_3$ gas diffusion oxygen electrodes. *J Solid State Electr* 18: 821–831.
38. Neburchilov V, Wang H, Martin JJ, et al. (2010) A review on air cathodes for zinc–air fuel cells. *J Power Sources* 195: 1271–1291.
39. Manoharan R, Shukla AK (1985) Oxide supported carbon/air electrodes for alkaline solutions power devices. *Electrochim Acta* 30: 205–209.
40. Karlsson G (1985) Perovskite catalysts for air electrodes. *Electrochim Acta* 30: 1555–1561.
41. Wang W, Huang Y, Jung S, et al. (2006) A Comparison of LSM, LSF, and LSCo for solid oxide electrolyzer anodes. *J Electrochem Soc* 153: A2066–A2070.
42. Patrakeev MV, Bahteeva JA, Mitberg EB, et al. (2003) Electron/hole and ion transport in $La_{1-x}Sr_xFeO_{3-\delta}$. *J Solid State Chem* 172: 219–231.
43. Tsipis EV, Kharton VV (2008) Electrode materials and reaction mechanisms in solid oxide fuel cells: a brief review. II. Electrochemical behavior vs. materials science aspects. *J Solid State Electr* 12: 1367–1391.
44. Sun C, Hui R, Roller J (2010) Cathode materials for solid oxide fuel cells a review. *J Solid State Electr* 14: 1125–1144.
45. Anderson MD, Stevenson JM, Simner SP (2004) Reactivity of lanthanide ferrite SOFC cathodes with YSZ electrolyte. *J Power Sources* 129: 188–192.
46. Kinoshita K (1992) *Electrochemical Oxygen Technology*, New York: John Wiley and Sons.
47. Wang J, Zhang Y, Guo W, et al. (2013) Electrochemical behavior of $La_{0.8}Sr_{0.2}FeO_3$ electrode with different porosities under cathodic and anodic polarization. *Ceram Int* 39: 5263–5270.
48. Bronoel G, Grenier JC, Reby J (1980) Comparative behavior of various oxides in the various electrochemical reactions of oxygen evolution and reduction in alkaline medium. *Electrochim Acta* 25: 1015–1018.
49. Bockris JOM, Otagawa T (1984) The electrocatalysis of oxygen evolution on perovskites. *J Electrochem Soc* 131: 290–302.

50. Wattiaux A, Grenier JC, Pouchard M, et al. (1987) Electrolytic oxygen evolution in alkaline medium of $La_{1-x}Sr_xFeO_{3-y}$ perovskite/related ferrites I. Electrochemical study. *J Electrochem Soc* 134: 1714–1724.
51. Suresh K, Panchapagesan TS, Patil KC (1999) Synthesis and properties of $La_{1-x}Sr_xFeO_3$. *Solid State Ionics* 126: 299–305.
52. Mo ϙoteguy P, Brisse A (2013) A review and comprehensive analysis of degradation mechanisms of solid oxide electrolysis cells. *Int J Hydrogen Energ* 38: 1587–15902.
53. Ramos T, Carvalho MD, Ferreira LP, et al. (2006) Structural and magnetic characterization of the series $La_{1-x}Sr_xFeO_3$. *Chem Mater* 18: 3860–3865.
54. Zafar A, Imran Z, Rafiq MA, et al. (2011) Evidence of Pool-Frenkel conduction mechanism in Sr-doped lanthanum ferrite $La_{1-x}Sr_xFeO_3$ ($0 \le x \le 1$) system. 2011 Saudi International Electronics, Communications and Photonics Conference (SIECPC).
55. Dann SE, Currie DB, Weller MT, et al. (1994) The effect of oxygen stoichiometry on phase relations and structure in the system $La_{1-x}Sr_xFeO_{3-\delta}$ ($0 \le x \le 1$, $0 \le \delta \le 0.5$). *J Solid State Chem* 109: 134–144.
56. Li XX, Qu W, Zhang JJ, et al. (2011) Electrocatalytic activities of $La_{0.6}Ca_{0.4}CoO_3$ and $La_{0.6}Ca_{0.4}CoO_3$-carbon composites toward the oxygen reduction reaction in concentrated alkaline electrolytes. *J Electrochem Soc* 158: A597–A604.
57. Staud N, Ross PN (1986) The corrosion of carbon black anodes in alkaline electrolyte II. Acetylene black and the effect of oxygen evolution catalysts on corrosion. *J Electrochem Soc* 133: 1079–1084.
58. Augustin CO, Selvan RK, Nagaraj R, et al. (2005) Effect of La^{3+} substitution on the structural, electrical and electrochemical properties of strontium ferrite by citrate combustion method. *Mater Chem Phys* 89: 406–411.
59. Trasatti S, Petrii O (1991) Real surface area measurements in electrochemistry. *Pure Appl Chem* 63: 711–734.
60. Miyahara Y, Miyazaki K, Fukutsuka T, et al. (2014) Catalytic roles of perovskite oxides in electrochemical oxygen reactions in alkaline media. *J Electrochem Soc* 161: F694–F697.
61. Mohamed R, Cheng X, Fabbri E, et al. (2015) Electrocatalysis of perovskites: The influence of carbon on the oxygen evolution activity. *J Electrochem Soc* 162: F579–F586.
62. Poux T, Napolsky FS, Dintzer T, et al. (2012) Dual role of carbon in the catalytic layers of perovskite/carbon composites for the electrocatalytic oxygen reduction reaction. *Catal Today* 189: 83–92.
63. Nishio K, Molla S, Okugaki T, et al. (2015) Effects of carbon on oxygen reduction and evolution reactions of gas-diffusion air electrodes based on perovskite-type oxides. *J Power Sources* 298: 236–240.
64. Matsumoto Y, Yoneyama H, Tamura H (1977) Catalytic activity for electrochemical reduction of oxygen of lanthanum nickel-oxide and related oxides. *J Electroanal Chem* 79: 319–326.
65. Parthasarathy A, Martin CR, Srinivasan S (1991) Investigations of the oxygen reduction reaction at the platinum nafion interface using a solid state electrochemical cell. *J Electrochem Soc* 138: 916–921.
66. Alegre C, Modica E, Aric ò AS, et al. (2017) Bifunctional oxygen electrode based on a perovskite/carbon composite for electrochemical devices. *J Electroanal Chem* [In Press].

67. Wang J, Zhao H, Gao Y, et al. (2016) $Ba_{0.5}Sr_{0.5}Co_{0.8}Fe_{0.2}O_{3-\delta}$ on N-doped mesoporous carbon derived from organic waste as a bi-functional oxygen catalyst. *Int J Hydrogen Energ* 41: 10744–10754.
68. Zhu Y, Zhou W, Yu J, et al. (2016) Enhancing electrocatalytic activity of perovskite oxides by tunning cation deficiency for oxygen reduction and evolution reactions. *Chem Mater* 28: 1691–1697.
69. Alegre C, Modica E, Rodlert-Bacilieri M, et al. (2017) Enhanced durability of a cost-effective perovskite-carbon catalyst for the oxygen evolution and reduction reactions in alkaline environment. *Int J Hydrogen Energ* [In Press].
70. Li X, Pletcher D, Russell AE, et al. (2013) A novel bifunctional oxygen GDE for alkaline secondary batteries. *Electrochem Commun* 34: 228–230.
71. Gorlin Y, Jaramillo TF (2010) A bifunctional nonprecious metal catalyst for oxygen reduction and water oxidation. *J Am Chem Soc* 132: 13612–13614.
72. Yuasa M, Yamazoe N, Shimanoe K (2011) Durability of carbon-supported La–Mn perovskite-base type of oxide for oxygen reduction catalysts in strong alkaline solutions. *J Electrochem Soc* 158: A411–A416.
73. Pourbaix M (1974) *Atlas of electrochemical equilibria in aqueous solution*, Houston, Tex, United States: National Association of Corrosion Engineers.
74. Karlson L, Lindström H (1986) Catalyst for oxygen evolution in bifunctional air-cathodes. *J Mol Catal* 38: 41–48.